Theoretical interpretation of the experimental electronic structure of lens-shaped self-assembled InAs/GaAs quantum dots

A. J. Williamson,* L. W. Wang, and Alex Zunger
National Renewable Energy Laboratory, Golden, Colorado 80401
(Received 3 March 2000)

We adopt an atomistic pseudopotential description of the electronic structure of self-assembled, lens-shaped InAs quantum dots within the ''linear combination of bulk bands'' method. We present a detailed comparison with experiment, including quantites such as the single-particle electron and hole energy level spacings, the excitonic band gap, the electron-electron, hole-hole, and electron-hole Coulomb energies and the optical polarization anisotropy. We find a generally good agreement, which is improved even further for a dot composition where some Ga has diffused into the dots.

I. USING THEORY AS A BRIDGE BETWEEN THE STRUCTURE AND ELECTRONIC PROPERTIES OF QUANTUM DOTS

Self-assembled, Stranski-Krastanow grown semiconductor quantum dots have recently received considerable attention as they exhibit a rich spectrum of phenomena including quantum confinement,[1–3] exchange splittings,[4] Coulomb charging/blockade,[5–13] and multiexciton transitions.[4,14] Over the past few years a considerable number of high-quality measurements of the electronic level structure of these dot systems have been performed, using photoluminescence (PL),[10,12,15–20] photoluminescence luminescence excitation,[4,14] capacitance,[5–7,13] and far infrared (FIR) spectroscopy.[7,21–26] These measurements have been able to determine the electronic level structure to relatively high precision. In parallel with these measurements, several groups have also attempted to measure the geometry and composition of these dots.[15,16,27–29] So far, however, these measurements have failed to provide details of the shape, size, inhomogeneous strain, and alloying profiles to a similar level of accuracy to that to which the electronic structure has been determined. As a result, the size of the dots were often used as adjustable parameters in models that fit experimental spectra. For example, using a single-band effective-mass model, Dekel *et al.*[14] defined an ''effective shape'' (cuboid) and ''effective dimension'' that reproduced the measured excitonic transitions. Similar ''parabolic dot'' models have been assumed by Hawrylak *et al.*[1]

The accuracy of single-band and multiband effective-mass methods was recently examined in a series of papers.[30–34] In these papers, the shape, size, and composition of nanostructures were arbitrarily fixed, and the electronic structure was evaluated by successively improving the basis set, starting from single-band methods (effective mass), going to six- and eight-band methods ($k.p$), and finally, using a converged, multiband approach (plane-wave pseudopotentials). It was found that conventional effective-mass and $k.p$ methods can sometimes significantly misrepresent the fully converged results even when the shape, size, and composition were given. The observed discrepancies were both quantitative (such as band-gap values, level spacings, Coulomb energies) and qualitative (absence of polarization anisotropy in square based pyramidal dots,[34] missing energy levels.[32]) As a result of these limitations these methods may not offer a reliable bridge between the electronic and atomistic structure.

In this paper, we offer a bridge between recent measurements of the *electronic structure* and measurements of the *atomic structure* of the dots using accurate theoretical modeling. Modeling can determine if the calculated electronic structure resulting from an assumed shape, size, strain, and alloying profiles agrees with the measured electronic structure or not. A theory that can perform such a ''bridging function'' must be accurate and reliable. The pseudopotential approach to this problem qualifies, in that any discrepancy between the predicted and measured electronic properties can be attributed to incorrectly assumed shape, size, or alloying profile. We have studied a range of shapes, sizes, and alloy profiles and find that a lens-shaped InAs dot with an inhomogeneous Ga alloying profile is in closest agreement with current measurements. In the following sections we attempt to provide a consistent theoretical interpretation of numerous spectroscopic properties of InAs/GaAs dots.

II. OUTLINE OF THE METHOD OF CALCULATION

We aim to calculate the energy associated with various electronic excitations in InAs/GaAs quantum dots. These energies can be expressed as total-energy differences and require four stages of calculation:

(i) *Assume the shape, size, and composition and compute the equilibrium displacements*: We first construct a supercell containing both the quantum dot and surrounding GaAs barrier material. The shape, size, and composition profile are taken as input and subsequently refined. Sufficient GaAs barrier is used, so that when periodic boundary conditions are applied to the system, the electronic and strain interactions between dots in neighboring cells are negligible. The atomic positions within the supercell are then relaxed by minimizing the strain energy described by an atomistic force field[35,36] including bond-bending, bond-stretching, and bond-bending/bond-stretching interactions (see Sec. III A). An atomic force field is similar to continuum elasticity approaches[36] in that both methods are based on the elastic constants, $\{C_{ij}\}$, of the

 ©2000 The American Physical Society

underlying bulk materials. However, atomistic approaches are superior to continuum methods in two ways, (a) they can contain anharmonic effects, and (b) they capture the correct point-group symmetry, e.g., the point-group symmetry of a square based, zinc-blende pyramidal dot is C_{2v}, since the $[110]$ and $[1\bar{1}0]$ directions are inequivalent while continuum methods,[36] find C_{4v}. More details of the atomistic relaxation are given in Sec. III A.

(ii) *Set up and solve the pseudopotential single-particle equation*: A single-particle Schrödinger equation is set up at the relaxed atomic positions, $\{\mathbf{R}_{n\alpha}\}$:

$$\hat{H}\psi_i(\mathbf{r}) = \left\{ -\frac{\beta}{2}\nabla^2 + \sum_{n\alpha} \hat{v}_\alpha(\mathbf{r}-\mathbf{R}_{n\alpha}) \right\} \psi_i(\mathbf{r}) = \epsilon_i \psi_i(\mathbf{r}). \tag{1}$$

The potential for the system is written as a sum of strain-dependent, screened atomic pseudopotentials v_α, that are fit to bulk properties extracted from experiment and first-principles calculations (see Sec. III B). The Schrödinger equation is solved by expanding ψ in a linear combination of bulk states ϕ_{nk}, from bands *n*, and *k*-points *k*,

$$\psi_i(\mathbf{r}) = \sum_{n,k} c_{n,k}^{(i)} \phi_{nk}(\mathbf{r}), \tag{2}$$

taken at a few strain values. The solution of Eqs. (1) and (2) provides the level structure and dipole transition matrix elements. More details on the solution of the Schrödinger equation are given in Sec. III C.

(iii) *Calculate the screened, interparticle many-body interactions*: The calculated single-particle wave functions are used to compute the electron-electron, electron-hole, and hole-hole direct, J_{ee}, J_{eh}, J_{hh}, and exchange K_{ee}, K_{eh}, K_{hh}, Coulomb energies (see Sec. III D).

(iv) *Calculate excitation energies as differences in total, many-particle energies*: For example, the difference between the total-energy $E_{11}[h_0^1 e_0^1]$ of a dot with a hole in level h_0 and an electron in level e_0 and the total-energy $E_{00}[h_0^0 e_0^0]$ of the unexcited dot is

$$E_{11}[h_0^1 e_0^1] - E_{00}[h_0^0 e_0^0] = (\epsilon_{e_0} - \epsilon_{h_0}) - J_{e_0 h_0} + 2K_{e_0 h_0}\delta_{S0}, \tag{3}$$

where (in the absence of spin-orbit coupling) $\delta_{S0}=1$ for triplet states, and 0 for singlet states. Analagous expressions exist for electron-addition experiments (see Sec. III D).

The main approximations involved in our method are (a) the fit of the pseudopotential to the experimental data for bulk materials is never perfect (see Table I) and (b) we neglect self-consistent iterations in that we assume that the screened pseudopotential drawn from a bulk calculation is appropriate for the dot. Our numerical convergence parameters are (i) the size of the GaAs barrier separating periodic images of the dots, and (ii) the number of bulk wave functions used in the linear combination of bulk bands (LCBB) expansion of the wave functions. To examine the effects of these approximations and convergences on the ultimate level of accuracy that can be obtained with our methodology we have first applied these methods to an InGaAs/GaAs quantum well (see Sec. III E), where experimental measurements of the shape, size,

TABLE I. Fitted bulk electronic properties for GaAs and InAs using the screened atomic pseudopotentials, in Eq. (7). The hydrostatic deformation potential of the band gap and Γ_{15v} levels are denoted by a_{gap} and $a_{\Gamma_{15v}}$. The biaxial deformation potential is denoted by b and the spin-orbit splittings at the Γ_{15v} and L_{1v} points are denoted by Δ_0 and Δ_1.

	GaAs		InAs	
Property	EPM	Expt.[a]	EPM	Expt.[a]
E_{gap}	1.527	1.52	0.424	0.42
$E_{X_{5v}}$	−2.697	−2.96	−2.330	−2.40
$E_{X_{1c}}$	1.981	1.98	2.205	2.34
$E_{X_{3c}}$	2.52	2.50	2.719	2.54
$E_{L_{3v}}$	−1.01	−1.30	−5.76	−6.30
$E_{L_{1c}}$	2.36	1.81	1.668	1.71
m_e^*	0.066	0.067	0.024	0.023
$m_{hh}^*[100]$	0.342	0.40	0.385	0.35
$m_{hh}^*[111]$	0.866	0.57	0.994	0.85
$m_{lh}^*[100]$	0.093	0.082	0.030	0.026
$a_{\rm gap}$	−7.88	−8.33	−6.79	−5.7
$a_{\Gamma_{15v}}$	−1.11	−1.0	−0.826	−1.0
b	−1.559	−1.7	−1.62	−1.7
Δ_0	0.34	0.34	0.36	0.38
Δ_1	0.177	0.22	0.26	0.27

[a]Reference 41.

composition, and transition energies are more established. We next describe the details of our method.

III. DETAILS OF THE METHOD OF CALCULATION

A. Calculation of equilibrium atomic positions for a given shape

To calculate the relaxed atomic positions within the supercell, we use a generalization of the original valence force field (G-VFF)[35] model. Our implementation of the VFF includes bond-stretching, bond-angle bending, and bond-length/bond-angle interaction terms in the VFF Hamiltonian. This enables us to accurately reproduce the C_{11}, C_{12}, and C_{44} elastic constants in a zinc-blende bulk material. We have also included higher-order bond-stretching terms, which lead to the correct dependence of the Young's modulus with pressure. The G-VFF total energy can be expressed as

$$\begin{aligned} E_{VFF} = & \sum_i \sum_j^{nn_i} \frac{3}{8}[\alpha_{ij}^{(1)}\Delta d_{ij}^2 + \alpha_{ij}^{(2)}\Delta d_{ij}^3] \\ & + \sum_i \sum_{k>j}^{nn_i} \frac{3\beta_{jik}}{8 d_{ij}^0 d_{ik}^0}[(\mathbf{R}_j-\mathbf{R}_i)\cdot(\mathbf{R}_k-\mathbf{R}_i) \\ & - \cos\theta_{jik}^0 d_{ij}^0 d_{ik}^0]^2 + \sum_i \sum_{k>j}^{nn_i} \frac{3\sigma_{ijk}}{d_{ik}^0}\Delta d_{ij} \\ & \times[(\mathbf{R}_j-\mathbf{R}_i)\cdot(\mathbf{R}_k-\mathbf{R}_i) - \cos\theta_{jik}^0 d_{ij}^0 d_{ik}^0], \end{aligned} \tag{4}$$

where $\Delta d_{ij} = [(R_i - R_j)^2 - d_{ij}^{0^2}]/d_{ij}^0$. Here $\mathbf{R}_i$ is the coordinate of atom *i* and d_{ij}^0 and the ideal (unrelaxed) bond distance between atom types of *i* and *j*. Also, θ_{jik}^0 is the ideal

TABLE II. Input G-VFF parameters α, β, and σ to Eq. (4) and their resulting elastic constants C_{11}, C_{12}, and C_{44}.

	α	β (10^3 dyne/cm)	σ	$\alpha^{(2)}$	C_{11}	C_{12} (10^{11} dyne/cm^2)	C_{44}
GaAs	32.153	9.370	−4.099	−105.	12.11	5.48	6.04
InAs	21.674	5.760	−5.753	−112.	8.33	4.53	3.80

(unrelaxed) angle of the bond angle $j-i-k$. The Σ^{nn_i} denotes summation over the nearest neighbors of atom i. The bond stretching, bond-angle bending, and bond-length/bond-angle interaction coefficients $\alpha_{ij}^{(1)}(\equiv\alpha)$, β_{jik}, and σ_{jik} are related to the elastic constants in a pure zinc-blende structure in the following way:

$$C_{11}+2C_{12}=\sqrt{\frac{3}{4d_0}}(3\alpha+\beta-6\sigma),$$

$$C_{11}-C_{12}=\sqrt{\frac{3}{d_0}}\beta,$$

$$C_{44}=\sqrt{\frac{3}{d_0}}\frac{[(\alpha+\beta)(\alpha\beta-\sigma^2)-2\sigma^3+2\alpha\beta\sigma]}{(\alpha+\beta+2\sigma)^2}. \quad (5)$$

The second-order bond-stretching coefficient $\alpha^{(2)}$ is related to the pressure derivative of the Young's modulus by dB/dP, where $B=(C_{11}+2C_{12})/3$ is the Young's modulus. Note that in the standard[35] VFF, which we have used previously,[37–39] the last terms of Eq. (4) are missing, so $\sigma=0$ in Eq. (5). Thus there were only *two* free parameters (α,β) and therefore three elastic constants could not, in general, be fit exactly. The G-VFF parameters and the resulting elastic constants are shown in Table II for GaAs and InAs crystals. For an InGaAs alloy system, the bond-angle and bond-length/bond-angle interaction parameters β, σ for the mixed cation Ga-As-In bond angle are taken as the algebraic average of the In-As-In and Ga-As-Ga values. The ideal bond angle θ_{jik}^0 is 109° for the pure zinc-blende crystal. However, to satisfy Vegas's law for the alloy volume, we find that it is necessary to use $\theta_{\text{Ga-As-In}}^0=110.5°$ for the cation mixed bond angle.

As a simple test of this G-VFF for alloy systems, we compared the relaxed atomic positions from G-VFF with pseudopotential LDA results for a (100) $(\text{GaAs})_1/(\text{InAs})_1$ superlattice where the c/a ratio is fixed to 1, but we allow energy minimizing changes in the overall lattice constant (a_{eq}) and the atomic internal degrees of freedom (u_{eq}). We find $a_{eq}^{LDA}=5.8612$ Å and $u_{eq}^{LDA}=0.2305$, while the G-VFF results are $a_{eq}^{G-VFF}=5.8611$ Å and $u_{eq}^{G-VFF}=0.2305$. In comparison the original VFF yields $a_{eq}^{VFF}=5.8476$ Å and $u_{eq}^{VFF}=0.2303$.

B. The empirical pseudopotential Hamiltonian

We set up the single-particle Hamiltonian as

$$\hat{H}=-\frac{\beta}{2}\nabla^2+\sum_{n\alpha}\hat{v}_\alpha(\mathbf{r}-\mathbf{R}_{n\alpha}), \quad (6)$$

where $\mathbf{R}_{n\alpha}$ is the G-VFF relaxed position of the nth atom of type α. Here $\hat{v}_\alpha(\mathbf{r})$ is a screened empirical pseudopotential for atomic type α. It contains a local part and a nonlocal, spin-orbit interaction part.

The local potential part is designed to include dependence on the local hydrostatic strain $\text{Tr}(\epsilon)$:

$$v_\alpha^{loc}(r;\epsilon)=v_\alpha^{eq}(r;0)[1+\gamma_\alpha\text{Tr}(\epsilon)], \quad (7)$$

where the γ_α is a fitting parameter. The zero strain potential $v_\alpha^{eq}(r;0)$ is expressed in reciprocal space q as

$$v(q)=a_0(q^2-a_1)/[a_2e^{a_3q^2}-1]. \quad (8)$$

The local hydrostatic strain, $\text{Tr}(\epsilon)$, for a given atom at $\mathbf{R}$ is defined as Ω_R/Ω_0-1, where Ω_R is the volume of the tetrahedron formed by the four atoms bonded to the atom at $\mathbf{R}$. Ω_0 is the volume of that tetrahedron in the unstrained condition. The need for explicit dependence of the atomic pseudopotential on strain in Eq. (7) results from the following: While the description in Eq. (6) of the total pseudopotential as a superposition of atomic potentials situated at specific sites $\{R_{n\alpha}\}$, does capture the correct local symmetries in the system, the absence of a self-consistent treatment of the Schrödinger equation deprives the potential from changing in response to strain. In the absence of a strain-dependent term, the volume dependence of the energy of the bulk valence-band maximum is incorrect. While self-consistent descriptions show that the volume deformation potential $a_v=dE_v/d\ln\Omega$ of the valence-band maximum is *negative* for GaAs, GaSb, InAs, InSb, and for all, Group-II-VI semiconductors, this qualitative behavior cannot be obtained by a non-self-consistent calculation that lacks a strain dependent pseudopotential.

To calculate the spin-orbit interaction, each wave function must be represented by spin-up and spin-down components. The additional term in the Hamiltonian, which describes the spin-orbit interaction, is implemented in q space as a matrix (between plane wave k_1 and k_2). More specifically, we have

$$\hat{H}_{SO}=\sum_l |l\rangle V_l^{SO}(\mathbf{r})\mathbf{L}\cdot\mathbf{S}\langle l|. \quad (9)$$

Here $|l\rangle$ is the projection operator of spatial angular momentum l, $\mathbf{L}$ is the spacial angular momentum operator $\mathbf{S}$ is the Dirac spin operator (matrix between spin-up and -down components), and $V_l^{SO}(\mathbf{r})$ is a potential representing the spin-orbit interaction due to relativistic effects of core electron states. In a plane-wave basis $|k_1\rangle$, and $|k_2\rangle$, $\hat{H}_{SO}$ can be rewritten as

TABLE III. Parameters for the GaAs and InAs screened atomic pseudopotentials, in Eq. (7). This potential requires a plane-wave cutoff of 5 Ryd.

Parameter	In	Ga	As (InAs)	As (GaAs)
a_0	644.13	432 960	26.468	10.933
b_1	1.512 6	1.784 2	3.031 3	3.090 5
a_2	15.201	18 880	1.246 4	1.104 0
a_3	0.353 74	0.208 10	0.421 29	0.233 04
a_4	2.182 1	2.563 9	0.0	0.0

$$\langle k_1|\hat{H}_{SO}|k_2\rangle = \sum_l \frac{4i\pi}{\Omega}(2l+1)\left[\frac{dP_l(\cos\theta_{k_1k_2})}{d\cos\theta_{k_1k_2}}\right](\hat{k}_1\times\hat{k}_2)\cdot\hat{S} \times\int_0^\infty V_l^{SO}(r)j_l(|k_1|r)j_l(|k_2|r)r^2dr. \quad (10)$$

Here, $\theta_{k_1k_2}$ is the angle between k_1 and k_2, Ω is the volume of the unit cell, and j_l is a spherical bessel function. In our calculations, we have only included the effects of $l=1$ (p states), and have used a Gaussian model for $V_l^{SO}(r)$.

In Eq. (6), the kinetic energy of the electrons has been scaled by a factor of β. The origin of this β term is as follows: In an accurate description of the crystal band structure, such as the GW method,[40] a general, spatially nonlocal potential $V(r,r')$, is needed to describe the self-energy term. In the absence of such a term, the occupied bandwidth of an inhomogeneous electron gas is too large compared to the exact many-body result. To a first approximation, however, the leading effects of this nonlocal potential $V(r,r')$, can be represented by scaling the kinetic energy. This can be seen by Fourier transforming $V(r,r')$ in reciprocal space q, then making a Taylor expansion of q about zero. We find that the introduction of such a kinetic-energy scaling, β, permits a simultaneous fit of both the effective masses and energy gaps. In this paper, we fit $\beta=1.23$ for both GaAs and InAs.

The pseudopotential parameters in Eqs. (7) and (8) were fitted to the bulk band structures, experimental deformation potentials and effective masses and first-principles calculations of the valence-band offsets of GaAs and InAs. The alloy bowing parameter for the GaInAs band gap (0.6 eV) is also fitted. The pseudopotential parameters are given in Table III and their fitted properties are given in Table I.[41] We see that unlike the LDA, here we accurately reproduce the bulk band gaps and the bulk effective masses. One significant difference in our parameter set, to that used in conventional $k.p$ studies, is our choice of a negative magnitude for the valence-band deformation potential a_v, which we have obtained from LAPW calculations.[42]

The present InAs and GaAs pseudopotentials have been systematically improved relative to our previous InAs and GaAs potentials,[37,38,43–45] although the functional form has remained the same. First, the pseudopotentials for InAs and GaAs used in Ref. 37, 44 did not include the spin-orbit interaction. In Refs. 38, 43 and 45 we used potentials that included the spin-orbit interaction, but were not able to simultaneously, accurately fit the electron effective and the zone-center band gap, due to the lack of the above β parameter. The potential used here is identical to that used in Refs. 44 and 34.

C. Calculating the single-particle eigenstates

One could use a straightforward expansion of the single-particle wave functions in a plane-wave basis set, as we have previously done in Refs. 37, 38, and 39. However, as was shown in Refs. 34, 44, and 46, a more economical representation is to use the LCBB method.[34,44,46] Within the LCBB the eigenstates of the pseudopotential Hamiltonian are expanded in a basis of bulk Bloch orbitals

$$\psi_i(\mathbf{r}) = \sum_s \sum_{n,k} c_{s,n,k}^{(i)} u_{s,n,k}(\mathbf{r}) e^{i\mathbf{k}\cdot r}, \quad (11)$$

where $u_{s,n,k}(\mathbf{r})$ is the cell periodic part of the bulk Bloch wave function for structure s, at the nth band and the kth k-point. These states form a physically more intuitive basis than traditional plane waves, therefore the number of bands and k points can be significantly reduced to keep only the physically important bands and k points (around the Γ point in this case). This method was recently generalized to strained semiconductor heterostructure systems[44] and to include to spin-orbit interaction.[45] In this paper we use a LCBB basis derived from four structures s. These structures are (i) unstrained, bulk InAs at zero pressure, (ii) unstrained, bulk GaAs at zero pressure, (iii) bulk InAs subjected to the strain value in the center of the InAs dot, and (iv) bulk InAs subjected to the strain value at the tip of the InAs dot. By interpolating the strain profile between these four structures, the basis is able to accurately describe all the strain in the system. The wave vectors $\{k\}$ used here include all allowed values within $16\pi/L$ of the zone center, where L is the supercell size. For calculations of electron states, the band indices n, include only the band around the Γ_{1c} point. For the hole states we also include the three bands around the Γ_{15v} point. This basis set produces single-particle energies that are converged with respect to basis size, to within 1 meV.

D. Constructing the energies of different electronic configurations

Using screened Hartree–Fock theory, the energy associated with loading N electrons into a quantum dot can be expressed[47] as

$$E_N = \sum_i (\epsilon_i + \Sigma_i^{pol})n_i + \sum_{i<j} (J_{ij}^{ee} - K_{ij}^{ee})n_i n_j, \quad (12)$$

where ϵ_i are the single-particle energies, Σ_i^{pol} are the polarization self-energies of the ith electron state, J_{ij}^{ee} and K_{ij}^{ee} are the direct and exchange Coulomb integrals between the ith and jth electronic states, and n_i are the occupation numbers ($\Sigma_i n_i = N$). As shown in Ref. 47, for free standing, colloidal quantum dots the dielectric constant inside the dot is dramatically different to that outside (vacuum) and hence the polarization self-energy, Σ_i^{pol}, is very significant (~ 1 eV). For self-assembled InAs dots embedded in GaAs, the dielectric constants of InAs and GaAs are similar ($\epsilon_\infty = 12.3, 10.6$) and we calculate this term as ~ 1 meV. The

resulting effect on single-particle energy *differences* is therefore a fraction of an meV and so we choose to neglect this term. The direct and exchange Coulomb energies, are defined as

$$J_{ij}=\int\int \frac{|\psi_i(\mathbf{r}_1)|^2|\psi_j(\mathbf{r}_2)|^2}{\bar{\epsilon}(\mathbf{r}_1-\mathbf{r}_2)|\mathbf{r}_1-\mathbf{r}_2|}d\mathbf{r}_1 d\mathbf{r}_2,$$

$$K_{ij}=\int\int \frac{\psi_i^*(\mathbf{r}_1)\quad \psi_i(\mathbf{r}_2)\psi_j^*(\mathbf{r}_2)\psi_j(\mathbf{r}_1)}{\bar{\epsilon}(\mathbf{r}_1-\mathbf{r}_2)|\mathbf{r}_1-\mathbf{r}_2|}d\mathbf{r}_1 d\mathbf{r}_2, \quad (13)$$

where $\bar{\epsilon}$ is a phenomenological, screened dielectric function[43] containing a Thomas-Fermi electronic component and an ionic component from Ref. 48. Our exchange automatically includes both short- and long-range components.

Denoting electron levels as $e_0,e_1,e_2,\ldots$, hole levels as $h_0,h_1,h_2,\ldots$, and the number of electrons and holes as N and M, the total energy E_{MN}, is

$$E_{MN}=\sum_i -\epsilon_{h_i}m_i+\sum_{i<j}(J_{ij}^{hh}-K_{ij}^{hh})m_i m_j+\sum_i \epsilon_{e_i}n_i$$
$$+\sum_{i<j}(J_{ij}^{ee}-K_{ij}^{ee})n_i n_j-\sum_{ij}(J_{ij}^{eh}-K_{ij}^{eh})n_i m_j, \quad (14)$$

where n_i and m_i are the electron and hole occupation numbers, respectively, and $\Sigma_i n_i=N$ and $\Sigma_i m_i=M$. Using Eq. (14), in the strong confinement regime where kinetic-energy effects dominate over the effects of exchange and correlation, the energy of a single exciton created by the excitation of an electron from hole state i to electron state j can be expressed as

$$E_{ij}^{exciton}=(\epsilon_{e_j}-\epsilon_{h_i})-J_{ji}^{eh}+K_{ji}^{eh}\delta_{S0}. \quad (15)$$

To study charged dots, if one assumes the electron states are occupied in order of increasing energy (Aufbau principle),[49] the total energy of a dot charged with N electrons, E_{0N}, is

$$E_{00}[e_0^0]=0,$$

$$E_{01}[e_0^1]=\epsilon_{e_0},$$

$$E_{02}[e_0^2]=2\epsilon_{e_0}+J_{e_0,e_0},$$

$$E_{03}[e_0^2e_1^1]=(2\epsilon_{e_0}+\epsilon_{e_1})+[J_{e_0,e_0}+2J_{e_0,e_1}]-K_{e_0,e_1},$$

$$E_{04}[e_0^2e_1^2]=(2\epsilon_{e_0}+2\epsilon_{e_1})$$
$$+[J_{e_0,e_0}+J_{e_1,e_1}+4J_{e_0,e_1}]-2K_{e_0,e_1}. \quad (16)$$

E. Quantum well tests

To test the above methods, we first calculated the energy levels in a quantum well, and compared the results with experiment. In Fig. 1(a), we compare the calculated electron-heavy-hole transition energies for a 96 Å $In_{0.24}Ga_{0.76}As$ quantum well inside a GaAs matrix. The peaks in the experimental spectra occur[50] at 1.275, 1.395, and 1.538 eV. Our calculated transitions occur at 1.290, 1.404, and 1.545 eV, respectively. Figure 1(b) compares the band gap of a $In_{0.22}Ga_{0.78}As$ quantum well as a function of its thickness. The measured band gaps[51] for quantum wells with thicknesses of 6 and 18 ML (monolayer) are 1.458 and 1.351 eV. Our calculated values are 1.466 and 1.366 eV.

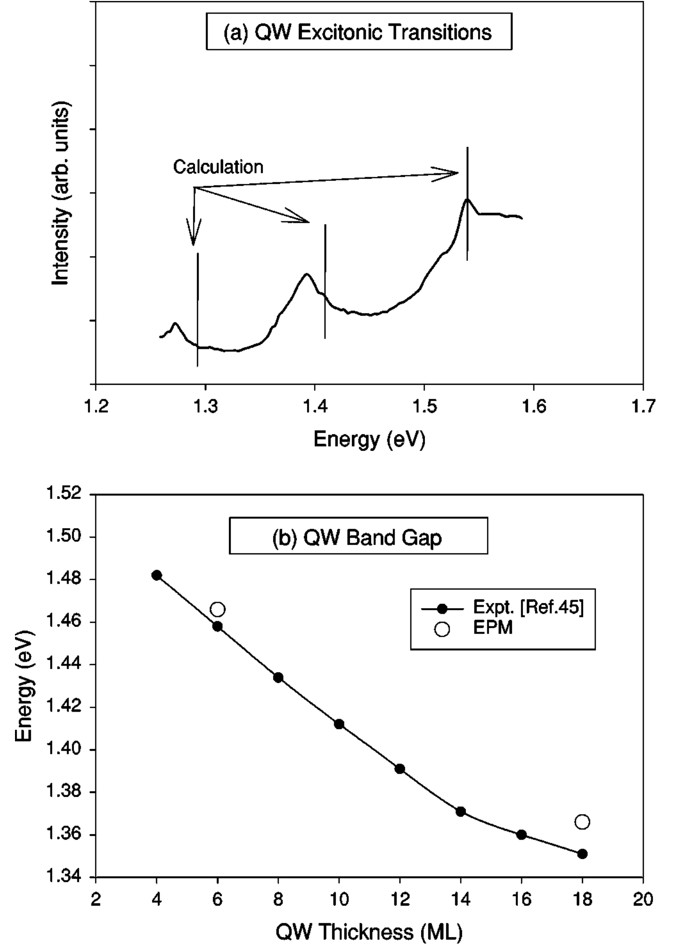

FIG. 1. (a) A comparison of EPM calculated and measured electron to heavy-hole transition energies in a 96 Å $In_{0.24}Ga_{0.76}As$ quantum well embedded inside a GaAs matrix. The vertical lines mark the positions of the EPM calculated transitions. (b) The calculated band gap of an $In_{0.22}Ga_{0.78}As$ quantum well as a function of its thickness.

IV. PHYSICAL QUANTITIES TO COMPARE WITH EXPERIMENT

The quantities we use to characterize the electronic structure are illustrated in Fig. 2, which shows a schematic layout of the electron and hole single-particle energy levels in a quantum dot. Assuming that all levels are spatially nondegenerate (thus having only spin degeneracy), we mark the electron levels as $e_0,e_1,e_2,\ldots$ and the hole levels as h_0, h_1, and h_2. The level e_0 is sometimes called "s-like," whereas e_1 and e_2 are called "p-like," and e_3 and e_4 are called "d-like." Since the GaAs environment of the InAs dots is largely unstrained, it is convenient to set as a reference energy the valence-band maximum (VBM) of GaAs as $E=0$, and the conduction band minimum (CBM) of GaAs as

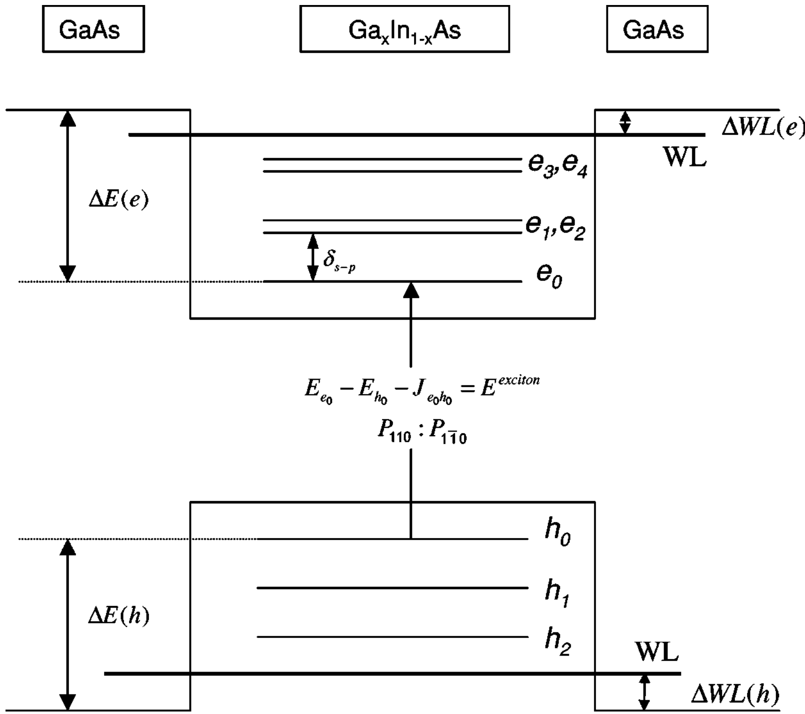

FIG. 2. Schematic single-particle electron and hole energy levels for lens-shaped, InAs quantum dots embedded within GaAs.

$E = 1520$ meV. All energy levels can be referenced with respect to these band edges.

For the *electron levels*, the quantities that we consider are (i) the number of dot-confined electron states, N_e, (ii) the spacing $\delta_{sp} = \epsilon_{e_1} - \epsilon_{e_0}$ between ''s-like'' and ''p-like'' electron states, (iii) the splitting $\delta_{pp} = \epsilon_{e_2} - \epsilon_{e_1}$ between the ''p-like'' electron states, (iv) the spacing $\delta_{pd} = \epsilon_{e_3} - \epsilon_{e_2}$ between ''p-like'' and ''d-like'' electron states, (v) the ''binding energy'' of the first electron level e_0, with respect to the GaAs conduction-band minimum, $\Delta E(e) = E_{\mathrm{GaAs},CBM} - \epsilon_{e_0}$, (vi) the position of the bottom of the band for the two-dimensional (2D) InAs ''wetting layer'' (WL) with respect to the GaAs CBM, $\Delta E_{WL}^{(e)} = E_{\mathrm{GaAs},CBM} - E_{WL}^{(e)}$, (vii) interelectron direct J_{e_i,e_j}^{ee} and exchange K_{e_i,e_j}^{ee} Coulomb energies.

For the *hole levels* we consider: (i) the number, N_h, of dot-confined hole states, (ii) the intraband spacings of the hole levels, $\delta_{ij}^{(h)} = \epsilon_{h_j} - \epsilon_{h_i}$, (iii) the ''binding energy'' of the first hole level h_0, with respect to the GaAs valence-band maximum, $-\Delta E(h) = E_{\mathrm{GaAs},VBM} + \epsilon_{h_0}$, (iv) The position of the top of the band for the 2D InAs WL with respect to the GaAs VBM, $\Delta E_{\mathrm{WL}}^{(h)} = -E_{\mathrm{GaAs},VBM} + E_{WL}^{(h)}$, (v) Interhole direct J_{h_i,h_j}^{hh} and exchange K_{h_i,h_j}^{hh} Coulomb energies.

Finally, for the *recombination of electrons and holes*, we consider:

(i) The excitonic energies, $E_{ij}^{exciton}$, as defined in Eq. (15). By subtracting calculated values for the single-particle energies ϵ_{e_j} and ϵ_{h_i} from measured optical excitation energies one can estimate the electron-hole direct Coulomb energies $J_{h_i e_j}$.

(ii) The ratio of absorption intensities for light polarized along the [110] and $[1\bar{1}0]$ directions, defined as

$$\lambda = \frac{P_{[110]}}{P_{[1\bar{1}0]}} = \frac{\langle \psi_{e_0} | r_{[110]} | \psi_{h_0} \rangle^2}{\langle \psi_{e_0} | r_{[1\bar{1}0]} | \psi_{h_0} \rangle^2}. \tag{17}$$

This ratio can deviate from unity due to three reasons; (a) The dots have different dimensions in the [110] and $[1\bar{1}0]$ directions. We refer to this as the geometric factor. (b) The atomistic zincblende symmetry makes the two directions symmetry inequivalent even if the lengths along the two directions are equal. We refer to this as the ''atomic symmetry factor.'' One manifestation of this affect is that if the strain is calculated atomistically, it is different in the two directions even in the absence of a geometric factor.[36] (c) A piezoelectric field that breaks the symmetry. Previous studies[16] have shown that this effect is negligible in InAs/GaAs dots so we will neglect it here. $k.p$ calculations neglect the ''atomic symmetry'' factor (except for the small effect of strain asymmetry), but retain the ''geometric factor.'' Pseudopotential calculations retain both effects. For example, in a *square* based pyramid (where by definition the ''geometric factor'' does not contribute), $k.p$ produces $\lambda = 1$, while pseudopotential theory gives $\lambda = 1.2$ (see Table IV). This shows that there is not a simple mapping from dot shape to polarization anisotropy λ.

(iii) Excitonic dipole: As the center of the electron and hole wave functions do not exactly coincide with each other, it is possible that an exciton will exhibit a detectable dipole moment,

$$d_{h_i,e_j} = \langle \psi_{h_i} | \hat{r} | \psi_{h_i} \rangle - \langle \psi_{e_j} | \hat{r} | \psi_{e_j} \rangle. \tag{18}$$

The quantities defined above characterize the electronic structure. Next, in Sec. V, we extract all of these quantities from our calculations, and in Sec. VI we extract measured values of these quantities from the available experiments.

V. THEORETICAL RESULTS

The electronic structure of a series of GaInAs/GaAs self-assembled quantum dots was calculated using the methodology described in Sec. II. We have chosen to focus on the

TABLE IV. Calculated single-particle electron and hole energy-level spacings, electron and hole binding energies, $\Delta E(e,h)$, electron-electron and electron-hole Coulomb energies, excitonic band gap all in meV, exciton dipole moment and polarization anisotropy for lens-shaped and pyramidal $Ga_xIn_{1-x}As$ quantum dots embedded within GaAs.

	Lens calculations						Pyramid calc.	Lens expt.
	(a)	(b)	(c)	(d)	(e)	(f)	(g)	
Geometry	252x35 Å	275x35 Å	252x25 Å	252x35 Å	252x35 Å	275x35 Å	200x100 Å	7,11
% Ga at base, tip, average	0,0,0	0,0,0	0,0,0	15,15,15	30,0,15	15,15,15	0,0,0	
$\delta_{sp}=e_1-e_0$	65	57	69	58	64	52	108	50
$\delta_{pd}=e_3-e_2$	68	61	67	60	63	57	64	48
$\delta_{pp}=e_2-e_1$	2	2	2	2	3	2	26	2
e_2-e_1(15T)	20	20	18	21	20	17		19
$\delta_{dd}=e_4-e_3$	4	3	4	4	3	1	23	
h_0-h_1	8	12	16	13	14	11	15	
h_1-h_2	7	6	5	5	6	5	20	
h_2-h_3	6	10	14	13	14	9	1	
$\Delta E(e)$	271	258	251	209	192	204	171	
$\Delta E(h)$	193	186	174	199	203	201	198	
$J_{e_0e_0}$	31	29	32	29	31	28	40	23
$J_{e_0e_1}$	25	24	26	24	24	24	35	24
$J_{e_1e_1}$	25	24	26	25	24	26	36	~18
$J_{h_0h_0}$	30	27	39	32	28	30	31	
$J_{e_0h_0}$	30	28	35	31	29	29	31	33.3
$K_{h_0e_0}$	0.15	0.13	0.14	0.15	0.1	0.12	0.2	
$e_0-h_0-J_{e_0h_0}$	1032	1016	1131	1080	1125	1083	1127	1098
d_{e_0,h_0} (Å)	0.16	−0.37	0.5	0.5	1.2	0.5	3.1	
$\lambda=P_{110}:P_{1\bar{1}0}$	1.03	1.01	1.04	1.05	1.08	1.08	1.20	

well-established ''lens-shaped'' dot geometry from Refs. 5–12. The shape of this dot is shown in Fig. 3. The profile is obtained by selecting the section of a pure InAs sphere that yields a circular base with diameter 252 Å and a height of 35 Å. The main experimental uncertainty about this dot is the composition profile. It is not known if the dots are pure InAs or if Ga has diffused into the dots. For comparison, we also calculate the electronic structure of a square based InAs pyramid with a base of 113 Å and a height of 56 Å. This is not believed to be a realistic geometry, however, it has been used as a benchmark for many previous theoretical calculations[34,37,38,52,53] and we include it here for comparison purposes. In the following sections these two geometries will be referred to as the ''lens'' and the ''pyramid.'' The results of our calculations are shown in Table IV and Fig. 4.

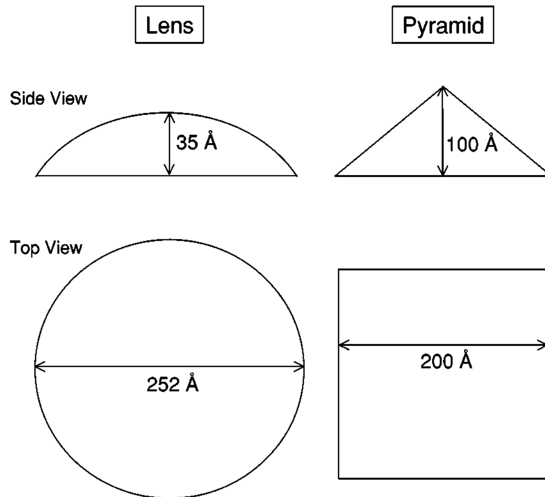

FIG. 3. Assumed model geometry of the lens- and pyramidal-shaped quantum dots.

A. Confined electron states

Figure 4 shows the calculated square of the envelope function for the electron states in the pyramidal- and lens-shaped InAs/GaAs quantum dots. For the lens-shaped dot, the electron states can be approximately interpreted as eigenstates of the $\hat{L}_z$ operator.[1] Here we plot only the first six bound states corresponding to $l_z=0$, ±1, and ±2. The first state e_0, has $l_z=0$ and is commonly described as *s*-like as it has no nodes. The e_1 and e_2 states have $l_z=\pm1$, and are *p*-like with nodal planes (110) and ($\bar{1}$10). The e_3, e_4, and e_5 states have $l_z=\pm2$ and 0, respectively, and are commonly described as $d_{x^2-y^2}$, d_{xy}, and $2s$, respectively. Due to the underlying zinc-blende atomistic structure, the C_∞ symmetry is reduced to C_{2v}. Hence, the e_0 to e_5 states correspond to the a_1, b_1, b_2, a_1, a_2, and a_1 irreducable representations of the C_{2v} group, rather than eigenstates of $\hat{L}_z$. This allows states e_0, e_3, and e_5 to couple. This coupling is evident, for example, in the larger charge density along [110] compared to $[1\bar{1}0]$ in the e_3 state, due to its coupling with e_1. The observable effect of this C_{2v} symmetry is to split the e_1 and e_2 *p* states, δ_{pp}, and the e_3 and e_4 *d* states, δ_{dd}. The alignment of the e_1 and e_2 *p* states along the [110] and $[1\bar{1}0]$ directions also results from the underlying zinc-blende lattice structure. Note, this analysis neglects the ef-

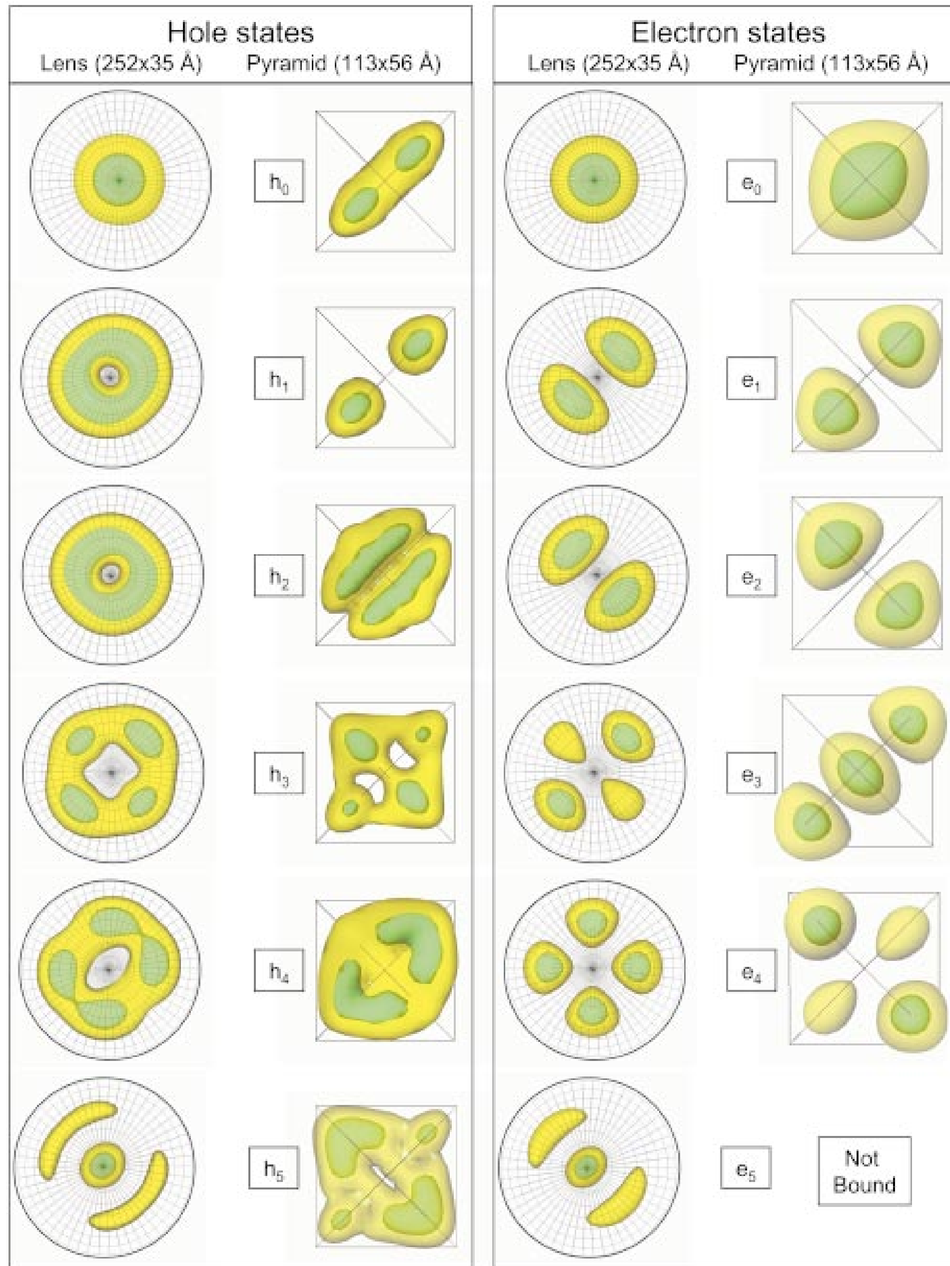

FIG. 4. (Color) Top view of the calculated electron and hole wave-functions squared for lens- and pyramidal-shaped InAs quantum dots embedded in GaAs, with bases of 252 and 113 Å and heights of 25 and 56 Å. The yellow and green isosurfaces represent 20% and 60% of the maximum charge density.

fects of the spin-orbit interaction, which reduces the C_{2v} group to a double group with the same single representation for all the states. In our calculations the spin-orbit interaction is included, but is produces no significant effects for the electron states.

The electron states in the pyramidal dot also belong to the C_{2v} group and show a one-to-one correspondence with those in the lens-shaped dot. However, there are only five bound states in the pyramidal dot due to its smaller size. Here we define an electron state as bound if its energy is below that of the unstrained, bulk GaAs conduction-band edge.

The calculated values of the s-p and p-d energy spacings, δ_{sp}, and, δ_{pd}, for the lens- and pyramidal-shaped dots, are 65 and 68 meV and 108 and 64 meV, respectively. The splitting of the two p states, $\delta_{pp}=e_2-e_1$ are 2 and 26 meV, respectively. The calculated values of the electron binding energy, $\Delta E(e)$, are 271 and 171 meV, respectively. The electron-electron direct Coulomb energies, $J^{ee}_{e_0e_0}$, $J^{ee}_{e_1e_1}$, and $J^{ee}_{e_0e_1}$ in the lens and pyramidal dots are calculated as 32, 25, and 25 meV and 40, 35, and 36 meV respectively. On applying a magnetic field in the growth direction, we calculate an increase in the splitting of the two p states (e_2-e_1) in the lens-shaped dot from 2 to 20 meV. Details of this magnetic-field calculation will be given in a future publication.[54] Finally, the energy of the electron wetting-layer level, $\Delta E^{(e)}_{\rm WL}$, with thicknesses of 1 and 2 ML, is 15 and 24 meV below the CBM of unstrained bulk GaAs.

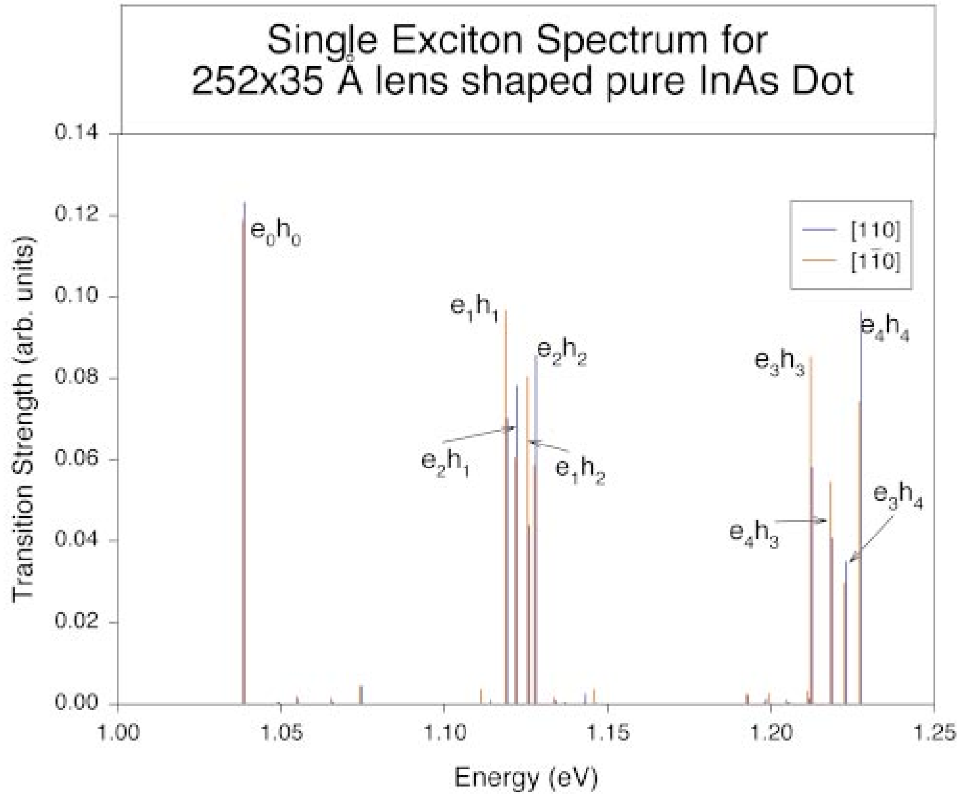

FIG. 5. (Color) The single exciton absorption spectrum for a pure InAs, lens-shaped dot with a base of 252 Å and a height of 35 Å. The absorption peaks are calculated from Eq. (15). The ratios of the dipole matrix elements for light polarized along [110] and [1$\bar{1}$0] are calculated from Eq. (17).

B. Confined hole states

Figure 4 shows calculated wave functions squared for the hole states in pyramidal- and lens-shaped InAs/GaAs quantum dots. Unlike the electron states, the hole states cannot be approximated by the solutions of a single band Hamiltonian. Instead there is a strong mixing between the original bulk Bloch states with Γ_{8v} and Γ_{7v} symmetry. The larger effective mass for holes results in a reduced quantum confinement of the hole states and consequently many more bound hole states. Only the six bound hole states with the highest energy are shown in Fig. 4.

The calculated values of the h_0-h_1, h_1-h_2, and h_2-h_3 hole level spacings for the pyramidal- and lens- shaped dots are 8, 7, and 6 meV and 15, 20, and 1 meV respectively. The calculated hole binding energies, $\Delta E(e)$, are 194 and 198 meV. We calculate the highest-energy hole level in pure InAs wetting layers, $\Delta E_{WL}^{(h)}$, with thicknesses of 1 and 2 ML to reside 30 and 50 meV above the VBM of unstrained bulk GaAs. The hole-hole Coulomb energies, $J_{h_0h_0}^{hh}$, are 25 and 31 meV.

C. Electron-hole excitonic recombination

Figure 5 shows our calculated single exciton absorption spectrum for a pure InAs, lens-shaped dot with a base of 252 Å and a height of 35 Å. The energies of each of the absorption peaks are calculated from Eq. (15). The ratios of the dipole matrix elements for light polarized along [110] and [1$\bar{1}$0] are calculated from Eq. (17). Figure 5 illustrates that, for a lens-shaped dot, both the conventional $e_i \rightarrow h_i$ transitions and additional e_1-h_2, e_2-h_1, e_3-h_4, and e_4-h_3 transitions are strongly allowed. The ratio of the polarization anisotropies λ are shown in Table V. As a result of the circular symmetry of the lens-shaped dot, we calculate a polarization ratio of $\lambda=1.03$ for the e_0-h_0 transition. This value is in contrast to that calculated value for a pyramidal dot of $\lambda=1.2$.[45] For the higher-angular momentum transitions we find larger deviations from unity. The magnitude of the ratios follows the polarization of the wave functions shown in Fig. 4. For example, we find ratios greater and then less than unity for the e_1-h_1 and e_2-h_2 transitions, as reflected by the elongations of the e_1,h_1 and e_2,h_2 wave functions along the [110] and [1$\bar{1}$0] directions.

We calculate ground-state electron-hole direct Coulomb energies, $J_{e_0h_0}^{eh}$, of 37 and 31 meV in the lens-shaped and

TABLE V. Calculated polarization anisotropy, $\lambda = P_{110}:P_{1\bar{1}0}$, for lens-shaped and pyramidal $Ga_xIn_{1-x}As$ quantum dots embedded within GaAs.

Geometry	Lens 252×35 Å	Pyramid 200×100 Å
% Ga at base, tip, average	0,0,0	0,0,0
e_0-h_0	1.03	1.20
e_1-h_1	0.82	2.40
e_2-h_2	1.27	0.52
e_3-h_3	0.73	4.26
e_4-h_4	1.23	0.63

pyramidal dots. The calculated ground-state electron-hole exchange energies, $K^{eh}_{e_0h_0}$ are an order of magnitude smaller, with values of 3 and 0.2 meV. These yield excitonic band gaps of 1.03 and 1.12, respectively. The calculated excitonic dipoles [Eq. (18)] are 3.1 and 0.16 Å, respectively. A positive dipole is defined as the center of the hole wave function being located above the center of the electron wave function.

VI. ANALYSIS OF PERTINENT EXPERIMENTAL MEASUREMENTS

A. The intraband *s-p* and *p-d* electron energy spacings

Measurements of the spacing between the e_0- and e_1-like electron levels (s-like and p-like) are based on infrared absorption. For the lens-shaped dots, Fricke *et al.*[7] load electrons into the dots by growing a sample consisting of an n-type doped layer, a tunneling barrier, a layer of InAs/GaAs lens-shaped dots, a GaAs spacer, and a GaAs/AlAs short period superlattice. By applying a voltage between the n-doped layer at the bottom of the sample and a Cr contact grown on top of the SPS, electrons are attracted from the n-doped layer into the InAs dots. Infrared photons were used to excite electrons from the occupied e_0 level into the e_1 level. Neglecting the small exchange energy, the energy differences for the e_1-e_0 excitations when one and two electrons are present in the dot are

$$E_{01}[e_1^1]-E_{01}[e_0^1]=(\epsilon_{e_1}-\epsilon_{e_0}),$$

$$E_{02}[e_0^1e_1^1]-E_{02}[e_0^2]=(\epsilon_{e_1}-\epsilon_{e_0})+[J^{ee}_{e_1,e_0}-J^{ee}_{e_0,e_0}]. \tag{19}$$

The first of these energy differences yields a direct measurement of the s-p energy spacing, δ_{sp}, of 49.1 meV. The second energy difference was measured at 50.1 meV. Drexler *et al.*[5] also used infrared transmission spectroscopy to measure an energy spacing, $\delta_{sp}=41$ meV. Pan *et al.*[21,26,22] have also performed infrared-absorption measurements on truncated pyramidal dots with a base of 180 Å and height of $\sim$60 Å. In these experiments, no gate voltage is applied, and therefore the excitations take place from the ground state of the samples, E_{00}. They observe multiple infrared- absorption peaks between 89 and 103 meV. These could be associated either with the s-p spacing of the electron levels or spacings of the hole states (see below).

Itskevich *et al.*[19] perform high-power PL measurements of pyramidal dots with a base of 150 Å and a height of 30 Å. This high-power excitation is able to simultaneously load multiple excitons into the dots. Due to state filling, these multiple excitons will occupy ground state (e_0,h_0) and higher (e_1,e_2,h_0,h_1,h_2) single-particle levels. Therefore the PL measurements are able to simultaneously measure recombination between electrons occupying the e_0, e_1, e_2, and e_3 levels with holes in the h_0, h_1, h_2, and h_3 levels. In general, to describe the total-energy differences associated with decay from N to $N-1$ excitons occupying a dot, requires a treatment that includes the exchange and correlation between multiple occupational configurations of the N and $N-1$ excitonic states. Such a configurational interaction approach has previously been considered for model parabolic dots[1] and will be discussed for realistic dots in a future publication.[55] For the purposes of this discussion, we limit ourselves to discussing the energy differences associated with the lowest-energy configurations on the N exciton state, i.e., those predicted by the Aufbau principle. Within this approximation, the peaks in the high-power, PL spectra can be interpreted as corresponding to [see Eq. (16) where exchange is neglected]

$$\text{Peak 1:}\quad E_{11}[h_0^1e_0^1]-E_{00}=(\epsilon_{e_0}-\epsilon_{h_0})-J^{eh}_{e_0,h_0},$$

$$\text{Peak 2:}\quad E_{33}[h_0^2h_1^1e_0^2e_1^1]-E_{22}[h_0^2e_0^2]=(\epsilon_{e_1}-\epsilon_{h_1})-J^{eh}_{e_1,h_1}+2[-J^{eh}_{e_1,h_0}-J^{eh}_{e_0,h_1}+J^{ee}_{e_1,e_0}+J^{hh}_{h_1,h_0}],$$

$$\text{Peak 3:}\quad E_{77}[h_0^2h_1^2h_2^2h_3^1e_0^2e_1^2e_2^2e_3^1]-E_{66}[h_0^2h_1^2h_2^2e_0^2e_1^2e_2^2]=(\epsilon_{e_3}-\epsilon_{h_3})-J^{eh}_{e_3,h_3}+2\sum_{i=0}^{2}[-J^{eh}_{e_3,h_i}-J^{eh}_{e_i,h_3}+J^{ee}_{e_3,e_i}+J^{hh}_{h_3,h_i}]. \tag{20}$$

Note, peak 3 is not assigned to a recombination from e_2 to h_2 as this is almost degenerate with peak 2. Itskevich *et al.* assume that (i) the Coulomb integrals in the square brackets on the right-hand side of Eq. (20) cancel, (ii) that $J^{eh}_{e_0,h_0}=J^{eh}_{e_1,h_1}=J^{eh}_{e_3,h_3}$, and (iii) that the hole spacings, $\delta_{h_0h_1}$, $\delta_{h_1h_2}$, are small compared to the electron level spacings. With these assumptions the spacings between peaks 1 and 2 and peaks 2 and 3 can be assigned to the s-p and p-d energy spacings. They find spacings δ_{sp} and δ_{pd} of 75 and 80 meV, respectively. Our calculations suggest that assumptions (i), (ii), and (iii) probably introduce errors of $\sim\pm10$, $\sim\pm5$, and $+10$ meV, respectively. The neglect of exchange interactions in the above discussion also introduces an error of $\sim\pm5$ meV.

B. The intraband electron *p*-level splitting

For the lens-shaped dots, the capacitance-voltage spectroscopy of Fricke *et al.*[7] can be used to estimate the splitting of the p states, δ_{pp}, by loading two electrons into the dot and exciting them using FIR spectroscopy. The relevant energy differences are

$$E_{02}[e_0^1e_1^1]-E_{02}[e_0^2]=(\epsilon_{e_1}-\epsilon_{e_0})+[J^{ee}_{e_1,e_0}-J^{ee}_{e_0,e_0}],$$

$$E_{02}[e_0^1 e_2^1]-E_{02}[e_0^2]=(\epsilon_{e_2}-\epsilon_{e_0})+[J^{ee}_{e_2,e_0}-J^{ee}_{e_0,e_0}]. \quad (21)$$

By assuming $J^{ee}_{e_1,e_0}=J^{ee}_{e_2,e_0}$, the difference in the two above expressions yields the energy spacing $\epsilon_{e_2}-\epsilon_{e_1}$. They find a value of ~2 meV. To measure the effect of a magnetic field on the splitting of the p states, Fricke *et al.*[7] use infrared absorption to measure the above energy differences in an applied magnetic field. At a field of 15 Tesla they measure an energy spacing of 19 meV.

C. The intraband hole energy spacings

In Ref. 23, Sauvage *et al.* used polarized photoinduced intraband absorption spectroscopy to measure the energy spacing between the lowest-hole state, h_{000}, and the hole state with a single node in the growth direction, h_{001}. This corresponds to [see Eq. (16)]

$$E_{11}[h^1_{000}e^1_0]-E_{11}[h^1_{001}e^1_0] =(\epsilon_{h_{001}}-\epsilon_{h_{000}})+[J^{eh}_{e_0,h_{000}}-J^{eh}_{e_0,h_{001}}]. \quad (22)$$

By assuming that $J^{eh}_{e_0,h_{000}}=J^{eh}_{e_0,h_{001}}$ Sauvage *et al.* estimate the h_{001}-h_{000} spacing to be ~120 meV. Note h_{001} is almost certainly higher in energy than states with nodes perpendicular to the growth direction due to the smaller dimension of the dot in the growth direction. Recently, Sauvage *et al.*[25] used midinfrared unipolar photoluminescence to measure additional hole splittings between h_0 and hole states with nodes perpendicular to the growth direction. The measured h_0-h_1 and h_1-h_2 splittings were 33 and 30 meV, respectively.

Tang *et al.*[56] measure activation energies for excitations from h_0 and h_1 to the hole wetting layer of 48 and 30 meV, respectively, implying an h_0-h_1 spacing of ~18 meV.

D. The electron and hole binding energies, $\Delta E(e)$ and $\Delta E(h)$

There have been no direct measurements of the electron or hole binding energy for lens-shaped InAs dots. However, it has been measured in other dots by several groups using a range of techniques. Berryman *et al.*[17] placed pyramidal InAs dots estimated to have a base of 100 Å and height of 15 Å in a p-n junction and measured the temperature dependence of the ac conductance as a function of frequency. These measurements predict a hole binding, $\Delta E(h)$, of ~240 meV. When subtracted from the bulk GaAs band gap, this yields a value for the electron binding energy, $\Delta E(e)$, of ~60 meV. The authors obtain similar results from temperature-dependent Hall measurements of thermal hole trapping. Itskevich *et al.*[18] measured the pressure at which PL measurements could detect a $\Gamma-X$ crossing in pyramidal InAs/GaAs quantum dot samples. By extrapolating these PL measurements back to zero pressure they were able to deduce a value for the electron binding energy, $\Delta E(e)$, of ~50 meV. Itskevich *et al.*[19] also used high-pressure PL to measure the energy difference between the X_{1c} level in bulk GaAs and the h_0 level in the quantum dots. By extrapolating this value back to zero pressure, they predict a value for the hole binding energy, $\Delta E(h)$, of ~250 meV. Brunkov *et al.*[13] performed capacitance-voltage spectroscopy measurements, which when fitted to a capacitance model for their dot geometry, predict an electron binding energy of 80 meV for dots with bases of 250 Å. Tang *et al.*[56] measured the spacing of the electron wetting layer to both the GaAs CBM and the e_0 level and hence deduced a value for the electron binding energy, $\Delta E(e)$, of ~80 meV, for dots with an estimated base of 130 to 170 Å.

E. The position of the electron and hole wetting-layer level

The presence of a distinct wetting-layer signal in the PL spectra of a sample of self-assembled quantum dots is the hallmark of a high-quality sample. In samples where the wetting layer has ''dissolved'' due to the growth conditions, it is likely that the geometry and composition of the quantum dots will also have dramatically altered from their uncapped state.

In the lens-shaped InAs dots, Schmidt *et al.*[10] observe PL emission from the ground state of the wetting layer at 1.34 eV. Photovoltage measurements[10] on the same samples show a strong peak corresponding to absorption into the ground state of the wetting layer at 1.35 eV. There are currently no measurements available for the position of the individual electron and hole wetting layers in the lens-shaped InAs/GaAs quantum dot samples. In Ref. 24, Sauvage *et al.* grow lens-shaped InAs dots with an estimated base of 150 Å and a height of 30 Å on a substrate that is n-doped with silicon. This n-doping loads electrons into the e_0 state in the dot, which they excite into the wetting layer using infrared excitation. In these samples they estimate the wetting layer to be 150 meV above the e_0 level. In Ref. 23 Sauvage *et al.* load electrons into the e_0 state of similar dots using an optical interband pump. Subsequent infrared absorption places the wetting layer 190 meV above the e_0 state. Tang *et al.*[56] measure thermal transfer of holes to the wetting layer, and obtain a spacing between the h_0 level and the hole wetting layer, $\Delta E^{(e)}_{WL}$ of ~48 meV. They also measure thermal transfer from an excited state, possibly involving h_1, which places the hole wetting layer ~30 meV below the h_1 level.

F. The number of confined electron and hole states

The actual number of confined electron and hole states in a self-assembled InAs/GaAs quantum dot depends on the size and composition of the dot. Early single band, effective-mass calculations[52] for pure InAs pyramidal dots with a base of 120 Å and height 60 Å predicted only a single bound electron state and several bound hole states. Consequently, many experiments were then interpreted in this light. More accurate multiband $k.p$[53,57,58] and pseudopotential[37,38] calculations have predicted five or more bound electron states in the same dots.

The high-power PL experiments of Itskevich *et al.*[19] show the gradual disappearance of five peaks as a function of external pressure. This is interpreted as direct evidence for five confined electron levels in their samples. The single dot, multiexciton measurements of Dekel *et al.*[14] require the assumption of at least three bound electron states to explain their experimental spectra. Similarly, the capacitance-voltage spectroscopy of Fricke *et al.*[7] shows two peaks corresponding to the capacitance of s-like states and the nearly degenerate p-like states, providing evidence for at least three bound electron states.

G. Electron and hole Coulomb and exchange interactions

By loading multiple electrons and holes into quantum dots it is possible to measure the Coulomb and exchange interactions between these additional electrons and holes. The magnitude of these interactions is a function of the shape of the electronic wave functions (see Sec. II) and provides an additional quantity to test the accuracy of theoretical models.

To study electron-electron interactions, Fricke *et al.*[7] use the same experimental setup discussed in Sec. VI A. From Eq. (16) we see the energy differences corresponding to the peaks in the capacitance voltage (CV) spectra associated with loading one and two electrons into the e_0 level in the dots is

$$E_{01}[e_0^1]-E_{00}=\epsilon_{e_0},$$

$$E_{02}[e_0^2]-E_{01}[e_0^1]=\epsilon_{e_0}+J^{ee}_{e_0,e_0}. \tag{23}$$

The electron-electron Coulomb interaction, $J^{ee}_{e_0,e_0}$, can therefore be directly measured as the splitting of these two CV peaks. They find a value of $J^{ee}_{e_0,e_0}\sim 23$ meV. From Eq. (19) we see that

$$J^{ee}_{e_0,e_1}=J^{ee}_{e_0,e_0}+(50.1-49.1)=24 \text{ meV}. \tag{24}$$

Finally by fitting four equidistant bell curves to the CV spectra corresponding to loading three, four, five, and six electrons into the dots, an approximate value for the charging energy between the p states, $J^{ee}_{e_1,e_1}$, of ~ 18 meV is obtained. From Eq. (16) we see that the spacing $E_{04}-E_{03}=J^{ee}_{e_1,e_1}+2J^{ee}_{e_0,e_1}$, while $E_{06}-E_{05}=3J^{ee}_{e_1,e_1}+2J^{ee}_{e_0,e_1}$ and hence the approximation of equidistant peaks will introduce some error into this estimate for $J^{ee}_{e_1,e_1}$.

H. Electron-hole excitonic recombination

To our knowledge, there have so far been no measurements of the polarization anisotropy in the lens-shaped dots discussed here. The polarization anisotropy for e_i-h_i excitonic recombination in InAs/GaAs was measured by Yang *et al.*,[15,16] for InAs dots formed by four $\{136\}$ faceted planes with bases ranging from 150 to 250 Å and a base to height ratio of 4:1. They found a ratio of $\lambda_{e_0,h_0}=1.2$ and $\lambda_{e_2,h_2}=1.3$. Yang *et al.*[15,16] performed $k.p$ calculations for this dot geometry, which include the "geometric factor" but not the "atomic symmetry factor" discussed in Sec. IV. They find $\lambda_{e_0,h_0}=1.8$ and $\lambda_{e_2,h_2}=3.5$. The authors suggest the $k.p$ simulations of the measured polarization ratio can be used to deduce the geometric shape anisotropy. However, we demonstrate here that when the atomic symmetry factor is included an anisotropy of $\lambda_{e_0,h_0}=1.3$ is obtained even for a *square* based pyramid. Thus $k.p$ simulations lacking the "atomic symmetry" factor cannot be used to reliably deduce the geometric shape anisotropy.

To our knowledge, there have so far been no measurements of the excitonic dipole in lens-shaped InAs dots. Fry *et al.*[20] used photocurrent spectroscopy within an applied electric field to measure the excitonic dipole moment, d_{h_i,e_j} [Eq. (18)]. They find the center of the hole wave functions to be located ~ 4 Å above the center of the electron wave function (positive dipole). Fry *et al.*[20] also perform single-band, effective-mass calculations, in an attempt to isolate the origin of this dipole. They predict that in the absence of alloying the dipole is -3 Å, i.e., the opposite sign, but a linear composition profile with $Ga_{0.5}In_{0.5}As$ at the base and pure InAs at the top of a truncated pyramid with a base of 155 Å, and height 55 Å, reproduces the correct dipole of 4 Å. They suggest that this alloying profile explains the observed dipole. We have repeated these calculations and confirm that, within a single-band model, such a composition profile causes both electrons and holes to move up in the dot compared to their positions in a pure InAs dot. The heavier effective mass of the holes, results in less kinetic energy associated with confinement at the top of the dot and hence the holes move up more than electrons on the introduction of Ga, producing the correct dipole. However, when we repeat these calculations in the more sophisticated, multiband LCBB basis used here, we find significant heavy hole-light hole mixing in the h_0 state, which acts to reduce the above effect and produce a smaller dipole of ~ 1 Å, in contradiction with experiment ($+4$ Å).

VII. COMPARISON OF EXPERIMENT AND THEORY

In Table IV we show the results of our calculations for pure InAs, lens-shaped quantum dots embedded within GaAs [column (a)]. Table IV also shows the experimentally measured splittings of the electron levels, the electron-electron, and electron-hole Coulomb energies, the magnetic-field dependence, and the excitonic band gap measured in Refs. 7 and 11. The agreement between the measured energy level spacings, Coulomb energies, and magnetic field-response with our theoretical lens-shaped model is generally good. Both the model and experiment find (i) a large spacing, δ_{sp}, ($\sim$50-60 meV) between the s-like e_0 state and the p-like e_1 state, (ii) a small spacing, δ_{pp},(~ 3 meV) between the two p-like e_1 and e_2 states, and (iii) a large spacing (~ 55 meV) between the p-like e_2 state and the d-like e_3 state.

These electron level spacings are similar to those found for pyramidal quantum dots[37] [see Table IV, column (g)]. However, in the pyramidal dot, the spacings of the two p-like and d-like states, δ_{pp}, δ_{dd}, are larger (26 and 23 meV). Both the model and experiment also find similar values for the Coulomb energies, $J(e_0e_0)$ and $J(e_0h_0)$ (~ 25 meV).

The calculated hole binding energy of $\Delta E(h)=193$ meV is in good agreement with those of Berryman *et al.*[17] (~ 240 meV) and Itskevich *et al.*[19] (~ 250 meV). Our calculated electron binding energies, $\Delta E(h)$, are considerable larger (271 meV) than those of Berryman *et al.*[17] (~ 60 meV) and Tang *et al.*[56] (~ 80 meV). We attribute this difference to the larger size of our dots. The assumption of a pure InAs dot also affects the comparison. The agreement improves when we include Ga in our dots (see Sec. VII B).

The calculated electron-electron and electron-hole Coulomb energies are in reasonable agreement with those extracted from Refs. 7 and 11. For the integrals $J^{ee}_{e_0e_0}$, $J^{ee}_{e_0e_1}$, $J^{ee}_{e_1e_1}$, and $J^{eh}_{e_0h_0}$ we calculate values of 31, 25,

25, and 37, respectively, compared to measured values of 23, 24, 18, and 33.3 meV.

The calculated polarization anisotropies, λ, for the e_0-h_0 recombination in lens and pyramidal shaped, pure InAs dots are $\lambda = 1.03$ and 1.2, respectively. A future measurement of this anisotropy ratio for lens-shaped dots would provide an important piece of evidence for determining the detailed geometry of the dots.

In the lens-shaped dot we find a difference in the average positions of the h_0 and e_0 states, d_{h_i,e_j}, of around 1 Å. This is smaller than the value we calculate for a pyramidal quantum dot, where we find the hole approximately 3.1 Å higher than the electron.

In summary, the assumed lens-shaped geometry, with a pure InAs composition produces a good agreement with measured level splittings, Coulomb energies, and magnetic-field dependence. A closer inspection of the remaining differences reveals that the calculations systematically *overestimate* the splittings between the single-particle electron levels (δ_{sp}: 65 vs 50 meV, δ_{pd}: 68 vs 48 meV) and *underestimate* the excitonic band gap (1032 vs 1098 meV).

A. Pure InAs dots: The effects of shape and size

Focusing on the lens shape only, we examine the effect of changing the height and base of the assumed geometry. Calculations were performed on similar lens-shaped, pure InAs dots where (i) the base of the dot was increased from 252 to 275 Å, while keeping the height fixed at 35 Å [column (b)], and (ii) the height of the dot was decreased from 35 to 25 Å, while keeping the base fixed at 252 Å [column (c)]. It shows that decreasing the height of the dot increases the quantum confinement and hence increases the splittings of the electron and hole levels (δ_{sp}: from 65 to 69 meV and δ_{h_0,h_1}: from 8 to 16 meV). Decreasing the height of the dot also acts to increase the excitonic band gap from 1032 to 1131 meV by pushing up the energy of the electron levels and pushing down the hole levels. Conversely, increasing the base of the dot decreases both the splittings of the single-particle levels (δ_{sp}: from 66 to 61 meV) and the band gap (1032 to 1016 eV). These small changes in the geometry of the lens-shaped dot have only a small effect on electronic properties that depend on the shape of the wave functions. The electron-electron and electron-hole Coulomb energies remain relatively unchanged, the magnetic-field induced splitting remain at 20 meV, the polarization anisotropy, λ, remains close to 1.0 and the excitonic dipole, d_{h_i,e_j}, remains negligible. In summary, reducing either the height or the base of the dot increases quantum confinement effects and hence increases energy spacings and band gaps, while not significantly effecting the wave functions.

B. Interdiffused In(Ga)As/GaAs lens-shaped dots

We next investigate the effect of changing the composition of the quantum dots, while keeping the geometry fixed. There have recently been several experiments[20,27,28] suggesting that a significant amount of Ga diffuses into the nominally pure InAs quantum dots during the growth process. We investigate two possible mechanisms for this Ga in-diffusion; (i) Ga diffuses into the dots during the growth process from all directions producing a dot with a uniform Ga composition $Ga_xIn_{1-x}As$, and (ii) Ga diffuses up from the substrate, as suggested in Ref. 20. To investigate the effects of these two methods of Ga in-diffusion on the electronic structure of the dots, we compare pure InAs dots embedded in GaAs with $Ga_xIn_{1-x}As$, random alloy dots embedded in GaAs, where the Ga composition, x, (i) is fixed at 0.15 [column (d)] and (ii) varies linearly from 0.3 at the base to 0 at the top of the dot [column (e)].

Table IV shows that increasing the amount of Ga in the dots acts to decrease the electron level spacings (δ_{sp}: from 65 to 58 for $x = 0.15$). It also acts to increase the excitonic band gap from 1032 to 1080 and 1125 meV, respectively. The electron binding energy, $\Delta E(e)$, is decreased by the in-diffusion of Ga (from 271 to 209 and 192 meV), while the hole binding energy, $\Delta E(h)$, is relatively unaffected. This significant decrease in the electron binding energy considerably improves the agreement with experiments on other dot geometries.[17,56]

As with changing the size of the dots, we find that Ga in-diffusion has only a small effects on properties that depend on the shape of the wave functions. The calculated electron-electron and electron-hole Coulomb energies are almost unchanged, while the average separation of the electron and hole, d_{h_i,e_j}, increases from 0.16 to to 0.5 and 1.2 Å and the polarization ratio, λ, and magnetic-field response are also unchanged.

Table IV shows that the dominant contribution to the increase in the excitonic band gap and reduction in electron binding energy results mostly from an increase in the energy of the *electron* levels as the Ga composition is increased. This can be understood by considering the electronic properties of the bulk $Ga_xIn_{1-x}As$ random alloy. The unstrained valence-band offset between GaAs and InAs is ~50 meV,[59] while the conduction-band offset in ~1100 meV and hence changing the Ga composition, x, has a large effect on the energy of the electron states and only a small effect on the hole states.

In summary, the effect of Ga in-diffusion is to reduce the spacing of the electron levels while significantly increasing their energy and hence increasing the band gap. We find that only the average Ga composition in the dots is important to their electronic properties. Whether this Ga is uniformly or linearly distributed throughout the dots has a negligible effect.

VIII. DISCUSSION

The effects of changing the *geometry* of the lens-shaped, pure InAs dots on the single-particle energy levels can be qualitatively understood from single-band, effective-mass arguments. These predict that decreasing any dimension of the dot, increases the quantum confinement and hence the energy-level spacings and the single-particle band gap will increase. Note that as the dominant quantum confinement in these systems arises from the vertical confinement of the electron and hole wave functions, changing the height has a stronger effect on the energy levels than changing the base.

As increasing (decreasing) the dimensions of the dot acts to decrease (increase) both the level spacings and the gap, it is clear that changing the dot geometry alone will not significantly improve the agreement with experiment as this requires a simultaneous *decrease* in the energy-level splittings and *increase* in the band gap. However, Ga in-diffusion into the dots acts to *increase* the band gap of the dot while decreasing the energy-level spacings.

Table IV shows that adopting a geometry with a base of 275 Å and a height of 35 Å and a uniform Ga composition of $Ga_{0.15}In_{0.85}As$ produces the best fit to the measurements in Refs. 7 and 11.

In conclusion, our results strongly suggest that to obtain very accurate agreement between theoretical models and experimental measurements for lens-shaped quantum dots, one needs to adopt a model of the quantum dot that includes some Ga in-diffusion within the quantum dot. When Ga in-diffusion is included, we obtain an excellent agreement between state of the art multiband pseudopotential calculations and experiments for a wide range of electronic properties. We are able to predict most observable properties to an accuracy of ± 5 meV, which is sufficient to make predictions of both the geometry and composition of the dot samples.

ACKNOWLEDGMENTS

We thank J. Shumway and A. Franceschetti for many useful discussions and their comments on the manuscript. This work was supported DOE—Basic Energy Sciences, Division of Materials Science under contract No. DE-AC36-99GO10337.

*Present address: Lawrence Livermore National Laboratory, Livermore, California 94550.

[1] L. Jacak, P. Hawrylak, and A. Wojs, *Quantum Dots* (Springer, Berlin, 1997).

[2] S. Gaponenko, *Optical Properties of Semiconductor Nanocrystals* (Cambridge University Press, Cambridge, 1998).

[3] A. Zunger, MRS Bull. **23**, 35 (1998).

[4] L. Landin, M. Miller, M.-E. Pistol, C. Pryor, and L. Samuelson, Science **280**, 262 (1998).

[5] H. Drexler, D. Leonard, W. Hansen, J. Kotthaus, and P. Petroff, Phys. Rev. Lett. **73**, 2252 (1994).

[6] D. Medeiros-Ribeiro, G. Leonard, and P. Petroff, Appl. Phys. Lett. **66**, 1767 (1995).

[7] M. Fricke, A. Lorke, J. Kotthaus, G. Medeiros-Ribeiro, and P. Petroff, Europhys. Lett. **36**, 197 (1996).

[8] B. Miller, W. Hansen, S. Manus, R. Luyken, A. Lorke, J. Kotthaus, S. Huant, G. Medeiros-Ribeiro, and P. Petroff, Phys. Rev. B **56**, 6764 (1997).

[9] R. Warburton, C. Durr, K. Karrai, J. Kotthaus, G. Medeiros-Ribeiro, and P. Petroff, Phys. Rev. Lett. **79**, 5282 (1997).

[10] K. Schmidt, G. Medeiros-Robeiro, J. Garcia, and P. Petroff, Appl. Phys. Lett. **70**, 1727 (1997).

[11] R. Warburton, B. Miller, C. Durr, C. Bodefeld, K. Karrai, J. Kotthaus, G. Medeiros-Ribeiro, P. Petroff, and S. Huant, Phys. Rev. B **58**, 16 221 (1998).

[12] K. Schmidt, G. Medeiros-Robeiro, and P. Petroff, Phys. Rev. B **58**, 3597 (1998).

[13] P. Brunkov, A. Suvorova, N. Vert, A. Kovsh, A. Zhukov, A. Egorov, V. Ustinov, N. Ledentsov, P. Kop'ev, and S. Konnikov, Semiconductors **32**, 1096 (1998).

[14] E. Dekel, D. Gershoni, E. Ehrenfreund, D. Spektor, J. Garcia, and P. Petroff, Phys. Rev. Lett. **80**, 4991 (1998).

[15] W. Yang, H. Lee, P. Sercel, and A. Norman, SPIE Photonics **1**, 3325 (1999).

[16] W. Yang, H. Lee, J. Johnson, P. Sercel, and A. Norman, Phys. Rev. B (to be published).

[17] K. Berryman, S. Lyon, and S. Mordechai, J. Vac. Sci. Technol. B **15**, 1045 (1997).

[18] I. Itskevich, S. Lyapin, I. Troyan, P. Klipstein, L. Eaves, P. Main, and M. Henini, Phys. Rev. B **58**, R4250 (1998).

[19] I. Itskevich, M. Skolnick, D. Mowbray, I. Troyan, S. Lyapin, L. Wilson, M. Steer, M. Hopkinson, L. Eaves, and P. Main, Phys. Rev. B **60**, R2185 (1999).

[20] P. Fry, I. Itskevich, D. Mowbray, M. Skolnick, J. Barker, E. O'Reilly, L. Wilson, I. Larkin, P. Maksym, M. Hopkinson, M. Al-Khafaji, J. David, A. G. Cullis, G. Hill, and J. C. Clark, Phys. Rev. Lett. **84**, 733 (2000).

[21] D. Pan, E. Towe, and S. Kennerly, Electron. Lett. **34**, 1019 (1998).

[22] D. Pan, E. Towe, S. Kennerly, and M.-Y. Kong, Appl. Phys. Lett. **76**, 3537 (2000).

[23] S. Sauvage, P. Boucaud, T. Brunhes, A. Lemaitre, and J.-M. Gerard, Appl. Phys. Lett. **71**, 2785 (1997).

[24] S. Sauvage, P. Boucaud, F. Julien, J.-M. Gerard, and V. Thierry-Mieg, Appl. Phys. Lett. **71**, 2785 (1997).

[25] S. Sauvage, P. Boucaud, T. Brunhes, A. Lemaitre, and J.-M. Gerard, Phys. Rev. B **60**, 15 589 (2000).

[26] D. Pan, E. Towe, and S. Kennerly, Appl. Phys. Lett. **73**, 1937 (1998).

[27] T. Metzger, I. Kegel, R. Paniago, and J. Peisl (private communication, 1999).

[28] J. Garcia, G. Medeiros-Ribeiro, K. Schmidt, T. Ngo, F. Feng, A. Lorke, J. Kotthaus, and P. Petroff, Appl. Phys. Lett. **71**, 2014 (1997).

[29] M. Rubin, G. Medeiros-Ribeiro, J. O'Shea, M. Chin, E. Lee, P. Petroff, and V. Narayanamurti, Phys. Rev. Lett. **77**, 5268 (1996).

[30] D. Wood and A. Zunger, Phys. Rev. B **53**, 7949 (1996).

[31] H. Fu and A. Zunger, Phys. Rev. Lett. **80**, 5397 (1998).

[32] L.-W. Wang and A. Zunger, J. Phys. Chem. **102**, 6449 (1998).

[33] C. Pryor, Phys. Rev. B **57**, 7190 (1998).

[34] L.-W. Wang, A. Williamson, A. Zunger, H. Jiang, and J. Singh, Appl. Phys. Lett. **76**, 339 (2000).

[35] P. Keating, Phys. Rev. **145**, 637 (1966).

[36] C. Pryor, J. Kim, L.-W. Wang, A. Williamson, and A. Zunger, J. Appl. Phys. **83**, 2548 (1998).

[37] J. Kim, L.-W. Wang, and A. Zunger, Phys. Rev. B **57**, R9408 (1998).

[38] A. Williamson and A. Zunger, Phys. Rev. B **59**, 15 819 (1999).

[39] A. Williamson and A. Zunger, Phys. Rev. B **57**, R4253 (1998).

[40] L. Hedin, J. Phys. C **11**, R489 (1999).

[41] Landolt and Borstein, *Numerical Data and Functional Relationships in Science and Technology, Vol. 22, Subvol. a* (Springer-Verlag, Berlin, 1997).

[42] A. Franceschetti, S.-H. Wei, and A. Zunger, Phys. Rev. B **50**, 17 797 (1994).

[43] A. Williamson and A. Zunger, Phys. Rev. B **58**, 6724 (1998).

[44] L.-W. Wang and A. Zunger, Phys. Rev. B **59**, 15 806 (1999).
[45] L.-W. Wang, J. Kim, and A. Zunger, Phys. Rev B **59**, 5678 (1999).
[46] L.-W. Wang, A.F. Franceschetti, and A. Zunger, Phys. Rev. Lett. **78**, 2819 (1997).
[47] A. Franceschetti, A. Williamson, and A. Zunger, J. Phys. Chem. (to be published).
[48] H. Haken, Nuovo Cimento **10**, 1230 (1956).
[49] A. Franceschetti and A. Zunger, Phys. Rev. Lett. **78**, 915 (1997).
[50] D. Gershoni, F. Vandenberg, S. Chu, G. Temkin, T. Tanbun-Ek, and R. Logan, Phys. Rev. B **40**, 10 017 (1989).
[51] J. Laymarie, C. Monier, A. Vasson, A.-M. Vasson, M. Leroux, B. Courboules, N. Grandjean, C. Deparis, and J. Massies, Phys. Rev. B **51**, 13 274 (1995).
[52] M. Grundmann, O. Stier, and D. Bimberg, Phys. Rev. B **52**, 11 969 (1995).
[53] M. Cusak, P. Briddon, and M. Jaros, Phys. Rev. B **54**, 2300 (1996).
[54] J. Shumway and A. Zunger (unpublished).
[55] A. J. Williamson, A. F. Franceschetti, and A. Zunger, Europhys. Lett. (to be published).
[56] Y. Tang, D. Rich, I. Mukhametzhanov, P. Chen, and A. Hadhukar, J. Appl. Phys. **84**, 3342 (1998).
[57] O. Stier, M. Grundman, and D. Bimberg, Phys. Rev. B **59**, 5688 (1999).
[58] H. Jiang and J. Singh, Appl. Phys. Lett. **71**, 3239 (1997).
[59] S.-H. Wei and A. Zunger, Appl. Phys. Lett. **72**, 2011 (1998).